SAND2011-8984C

THERMAL CONDUCTIVITY MANIPULATION IN SINGLE CRYSTAL SILICON VIA LITHOGRAPHYCALLY DEFINED PHONONIC CRYSTALS

Bongsang Kim[1], Janet Nguyen[1], Peggy J. Clews[1], Charles M. Reinke[1], Drew Goettler[2], Zayd C. Leseman[2], Ihab El-Kady[1, 2], and Roy H. Olsson III[1]

[1]Sandia National Laboratories, Albuquerque, NM, USA

[2]University of New Mexico, Albuquerque, NM, USA

ABSTRACT

The thermal conductivity of single crystal silicon was engineered to be as low as 32.6W/mK using lithographically defined phononic crystals (PnCs), which is only one quarter of bulk silicon thermal conductivity [1]. Specifically sub-micron through-holes were periodically patterned in 500nm-thick silicon layers effectively enhancing both coherent and incoherent phonon scattering and resulting in as large as a 37% reduction in thermal conductivity beyond the contributions of the thin-film and volume reduction effects. The demonstrated method uses conventional lithography-based technologies that are directly applicable to diverse micro/nano-scale devices, leading to potential performance improvements where heat management is important.

INTRODUCTION

The importance of heat management is rapidly growing in many micro/nano-mechanical devices. For instance, thermal actuation is one of the most widely used transducer mechanisms in MEMS devices, where large actuation forces or large displacement are needed [2]. Recently demonstrated ovenized micromechanical resonators use localized heating to address temperature induced frequency drift [3]. Micromachined thermoelectric converters are promising for next generation energy harvesters, generating electrical power from waste heat [4]. In such applications, effective heat management is critical to guarantee optimized performance.

However, in many cases, the issues of heat transfer are often coupled with the electrical conduction, complicating the situation. For instance, in the ovenized resonators demonstrated in [3], to enhance oven energy efficiency, high thermal isolation of the device from the surroundings is required; however, at the same time, for lower loss and noise, high electrical conductivity is desirable. In thermoelectric energy scavengers, their figure of merit, ZT, is proportional to the ratio between the electrical and thermal conductivity values. For maximum energy harvesting efficiency, high electrical conductivity and simultaneously low thermal conductivity are required. In general, however, these two conductivities track each other; if thermal conductivity decreases, electrical conductivity also decreases, and vice versa; therefore, thermal management paired with the electrical connectivity issue is not a trivial problem.

The manipulation of phonons is an effective way to deal with the heat transfer problem in micro/nano-scale devices. Unlike metals, where both electricity and heat are conducted through electrons, in many semiconductor materials, such as silicon, electrical conduction occurs through electrons while heat conduction is dominated by phonons, where the thermal energy is transferred through the vibration of the adjacent atomic lattices. In silicon, for instance, phonons of frequencies ranging from GHz to THz account for the majority of heat conduction [5]. Therefore, in such materials, if only phonons can be controlled, it is possible to manipulate thermal conductivity independently without altering the electrical conductivity.

There are two approaches to control phonon transfer and manipulate heat conduction presented in this work. The first is enhancing phonon scattering by reducing feature sizes. As the size of thermal pathways becomes comparable to the phonon mean-free-path, heat transfer can be significantly impacted, as has been frequently observed in small-scale structures such as thin-film deposited silicon and nano-wires [1,6]. The second method is phonon dispersion modification using periodically variant acoustic media (i.e. phononic crystals or PnCs). Phononic crystals can change the dispersion relation of phonons, modulating the phonon energy-carrying efficiency (or group velocity) so that the thermal conductivity is altered. Also by creating phononic bandgaps [7], a band of frequencies for which phonon propagation is forbidden, phonons at the frequencies responsible for heat transfer can be redistributed. The former is called incoherent phonon scattering and the latter is called coherent phonon scattering.

Previously, we have demonstrated effective phonon manipulation using lithographically defined phononic crystals [8]. Such lithography-based technology has huge potential because it allows direct application to many existing micro/nano-mechanical devices with very little modification to their original fabrication processes. In this work, using lithography-based phononic crystals, we demonstrate the ability to control thermal conductivity in single crystal silicon. Specifically, by periodically placing sub-micron through-holes, both incoherent and coherent phonon scattering could be effectively enhanced leading to a significant reduction in thermal conductivity, while leaving its electrical conductivity almost unaltered.

DESIGN AND FABRICATION

Figure 1 illustrates the test structure design for pho-

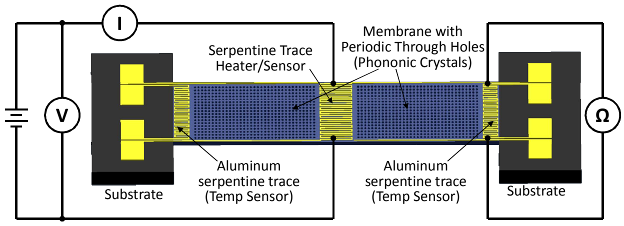

Figure 1. A schematic of the thermal conductivity measurement test structure and the test setup.

This work was supported by the Laboratory Directed Research and Development (LDRD) program at Sandia National Laboratories. Sandia National Laboratories is a multi-program laboratory operated by the Sandia Corporation, Lockheed Martin Company, for the United States Department of Energy's National Nuclear Security Administration under contract DE-AC04-94AL85000.

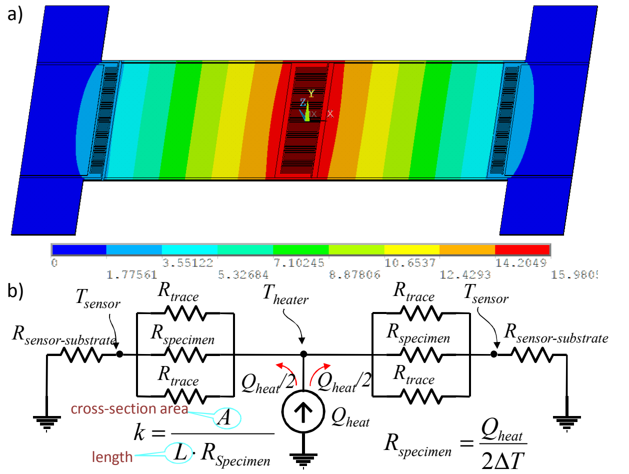

Figure 2. Equivalent a) ANSYS finite element simulation mo model and b) thermal circuit model of the test structure.

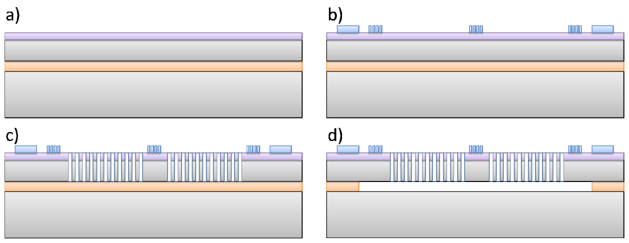

Figure 3. Fabrication process flow schematics (cross section view).Only conventional surface micromachining techniques were used to construct phononic crystals.

nonic crystal thermal conductivity measurements. A phononic crystal bridge containing periodic through-holes is suspended from the substrate by two anchors at the ends. A 250µm-wide aluminum serpentine trace functioning both as a heater and a temperature sensor is placed in the bridge center. To investigate device thermal characteristics, heat is supplied at the center and the temperature difference across the bridge is measured. Figure 2 shows the ANSYS FE-simulated thermal model and the equivalent thermal circuit model of the test structures. In these models, convection and radiation heat transfer is ignored. The complete design sets of hole diameters (D) and hole pitches (lattice constants, a), as well as the corresponding limiting dimensions (L) for the test structures are listed in Table 1.

The test structure fabrication process is illustrated in Figure 3. The fabrication begins with 6-inch SOI wafers, with the device layer composed of 500nm-thick lightly p-type doped (boron 10^{16}) single crystal silicon. On top of the single crystal silicon layer, 100nm of undoped amorphous silicon is deposited as an electrical isolation

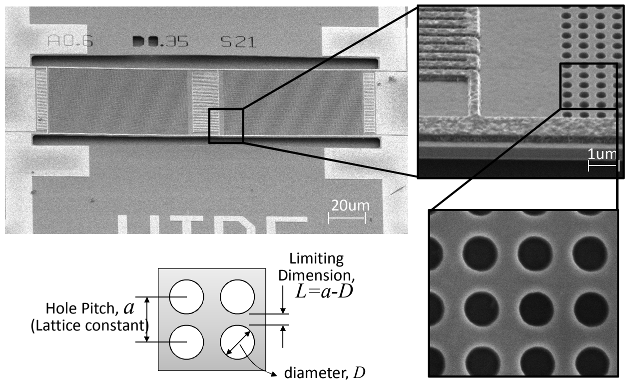

Figure 4. SEM images of fabricated test structures.

layer between the underlying device layer and the following metal layer (Figure 3a). The high stress in the amorphous silicon layer is released via high temperature annealing. Aluminum is deposited and patterned for heaters, temperature sensors, interconnects, and bondpads (Figure 3b). Phononic crystals and release trenches are defined in the silicon layers using an ASML UV stepper followed by plasma etching (Figure 3c). Finally, by timed HF vapor etching of the buried oxide (SiO_2) layer, the bridge-shaped test structure is released (Figure 3d). Figure 4 shows the SEM images of fabricated test structures.

MEASUREMENT

In a separate heated chuck measurement, the temperature dependence of the aluminum trace resistances was calibrated. Both traces were measured to have an almost identical relative resistance change due to temperature change, with the measured TCR (temperature coefficient of resistance) of

$$TCR = \frac{\Delta R / R}{\Delta T} = 0.0027 \quad (1)$$

To measure the device thermal resistance, the test setup shown in Figure 1 was used. While heat was supplied by applying power across the aluminum trace at the bridge center, the amount of heating power and trace resistance were extracted by measuring the voltage across the heater and the current through the trace. Simultaneously, the resistance changes of the sensor serpentine traces at the bridge ends were also measured. Using equation (1), the temperature shifts of the heater and sensors were calculated, while the heating power was swept from 0 to 1 mW and back to 0 again. All measurements were conducted in vacuum (< 1mTorr) to minimize convectional heat leakage. From the measured data, using the thermal models shown in Figure 2, the thermal resistances across the phononic

Table 1. Summary of phononic crystal design parameters and measured thermal conductivities and electrical conductivities. For each phononic crystal design (hole pitch and diameter combination), a total number of 6 devices were measured. Design ID-1 is the control device which doesn't have any holes in the membrane. Thermal conductivity values are at 300K.

Design ID	**1**	**2**	**3**	**4**	**5**	**6**	**7**	**8**	**9**	**10**	**11**	**12**	**13**	**14**	**15**	**16**	**17**
lattice constant, a (nm)	N/A	500	500	600	600	600	700	700	700	700	700	800	800	800	800	800	900
diameter, D (nm)	N/A	213	303	204	295	365	209	294	360	424	486	290	357	419	479	535	532
limiting dimension,L(nm)	N/A	286	196	395	304	234	491	405	339	275	213	509	442	380	320	265	367
mean k_m (W/mK)	104	63.3	42.4	73.7	56.3	42.8	79.4	65.7	54.1	43.3	32.6	72.2	63.4	53.5	44.4	35.8	45.1
standard dev. k_m (W/mK)	1.4	1.3	1.6	1.5	1.3	1.4	1.0	1.4	1.2	1.4	1.3	1.1	1.1	1.1	1.2	1.2	1.0
σ_m (S/cm)	1.849	1.377	0.983	1.522	1.234	0.990	1.598	1.382	1.197	1.004	0.802	1.484	1.342	1.186	1.029	0.875	1.050
$k_{relative} = k_m / k_{m,control}$	1	0.608	0.408	0.708	0.541	0.412	0.763	0.632	0.520	0.416	0.313	0.694	0.609	0.514	0.427	0.344	0.434
$\sigma_{relative} = \sigma_m / \sigma_{m,control}$	1	0.744	0.532	0.823	0.668	0.535	0.864	0.747	0.647	0.543	0.434	0.802	0.726	0.641	0.556	0.473	0.568
ζ_{FEM}	1	0.750	0.551	0.834	0.679	0.547	0.871	0.757	0.655	0.551	0.447	0.813	0.729	0.645	0.558	0.478	0.568
mean k_n	1	0.805	0.736	0.844	0.790	0.747	0.871	0.829	0.787	0.750	0.696	0.847	0.83	0.792	0.759	0.714	0.759
standard dev. k_n	0	0.006	0.017	0.008	0.007	0.013	0.008	0.009	0.007	0.013	0.017	0.007	0.003	0.005	0.009	0.013	0.007

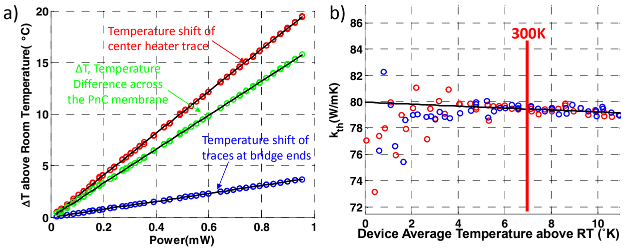

Figure 5. a) An example plot of the measured temperature vs. heating power plot (Design ID-7). The temperature difference across the phononic crystal bridge was measured using calibrated serpentine traces while the heating power supplied at the bridge center was swept between 0 to 1mW. b) An example plot of the measured thermal conductivity vs. device average temperature. For the consistency, the values at 300K were used for the data analysis.

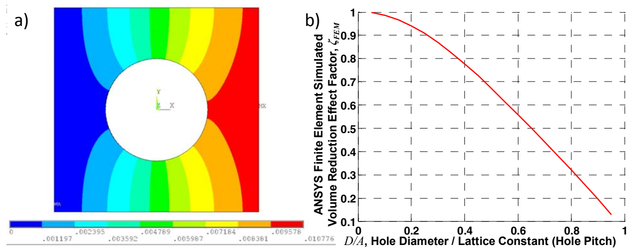

Figure 6. a) ANSYS finite element simulation of the effective conductivity reduction by introducing periodic through holes. This model captures only classical volume reduction effects, not any phononic effects. b) Volume reduction effect factors, ζ_{FEM}, vs. hole diameter/lattice constant.

crystal membrane and the corresponding thermal conductivities, k_m, were extracted. Figure 5 shows example plots of measured temperature rise vs. supplied heating power and measured thermal conductivity vs. average device temperature. All of the measured thermal conductivity data is summarized in Table 1. For consistency, the values at 300K were compared in this study. Electrical conductivities of the identical phononic crystal designs were also measured separately with n-type doped samples (phosphorus, 10^{19}) and summarized in Table 1 as well.

RESULT AND DISCUSSION

As can be seen in Table 1, all the samples containing holes (phononic crystals) showed a significant reduction in thermal conductivity as compared to the control device (Design ID-1), which did not have any holes. However, to understand the real phononic effect, the amount of reduction in thermal conductivity coming from the volume reduction effect by introducing the through holes has to be decoupled from these measured values.

To evaluate the volume reduction effect, ANSYS FE simulation models were used, as shown in Figure 6a. Since this ANSYS simulation only models continuum effects (Fourier's law for the thermal conductivity and Ohm's law for the electrical conductivity), and not any phonon scattering effects, the absolute dimension does not impact the result; only material porosity and the relative ratio between the hole size and pitch effects the thermal conduction. Figure 6b plots the FE simulated volume reduction effect factor, ζ_{FEM}, as a function of the material porosity.

Table 1 and Figure 7 compare relative thermal conductivities and relative electrical conductivities as well

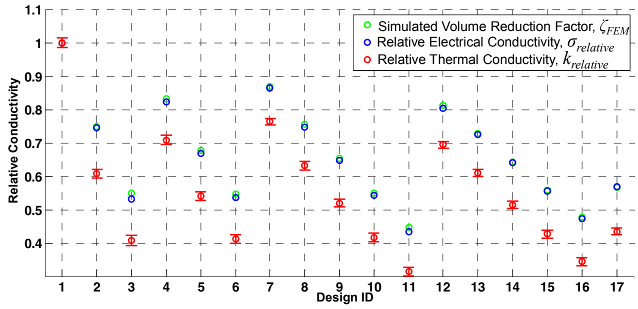

Figure 7. Comparison between $k_{relative}$ (at 300K), $\sigma_{relative}$, and ζ_{FEM}. The measured $\sigma_{relative}$ matches very well with ζ_{FEM} for all Design IDs. For some data points it is not easy to tell the difference because they exactly overlap with each other. However, $k_{relative}$ is much smaller than ζ_{FEM} for all cases, inferring a reduction in the thermal conductivity is beyond the contribution from the volume reduction effect.

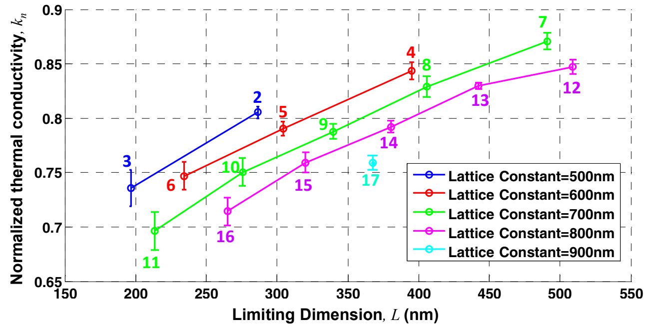

Figure 8. Comparison of k_n versus limiting dimension, L, with the same lattice constant, a. As the limiting dimension decreases, the k_n decreases, which indicates that incoherent phonon scattering plays a significant role to reduce thermal conductivity of the phononic crystals. Numbers adjacent the data points are the Design ID in Table 1.

as the ANSYS FE modeled volume reduction effect factors for each phononic crystal design. Here, the relative thermal conductivity and electrical conductivity were defined as,

$$k_{relative} = k_m / k_{m,control} \qquad (2\text{-}1)$$

$$\sigma_{relative} = \sigma_m / \sigma_{m,control} \qquad (2\text{-}2)$$

where, k_m and σ_m are the measured thermal and electrical conductivities respectively, and $k_{m,control}$ and $\sigma_{m,control}$ are the measured thermal and electrical conductivities of the control device (Design ID-1) respectively. As can be seen in Figure 7, for all samples, the relative thermal conductivities were measured much lower than the predictions of the volume reduction effect. In contrast, the relative electrical conductivities match very well with the FE simulated predictions of the corresponding phononic crystal designs. These results suggest that the inclusion of sub-micron periodic holes reduced the thermal conductivity significantly beyond the contribution from the volume reduction effect, whereas the electrical conductivity was reduced simply by the amount of volume reduction.

To evaluate the phononic effect on thermal conductivity more precisely, all measured relative thermal conductivities were again normalized by the simulated volume reduction factors, i.e.,

$$k_n = \frac{k_{relative}}{\zeta_{FEM}} = \frac{k_m / k_{m,control}}{\zeta_{FEM}} \qquad (3)$$

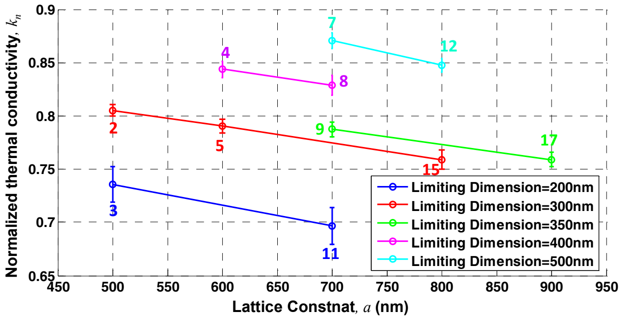

Figure 9. Comparison of k_n versus lattice constant, a, with the same limiting dimensions. Even with the same limiting dimension, k_n consistently decreases as the lattice constant increases. These differences in k_n indicate that incoherent scattering is not the only mechanism contributing to the reduction in thermal conductivity. Numbers adjacent the data points are the Design ID in Table 1.

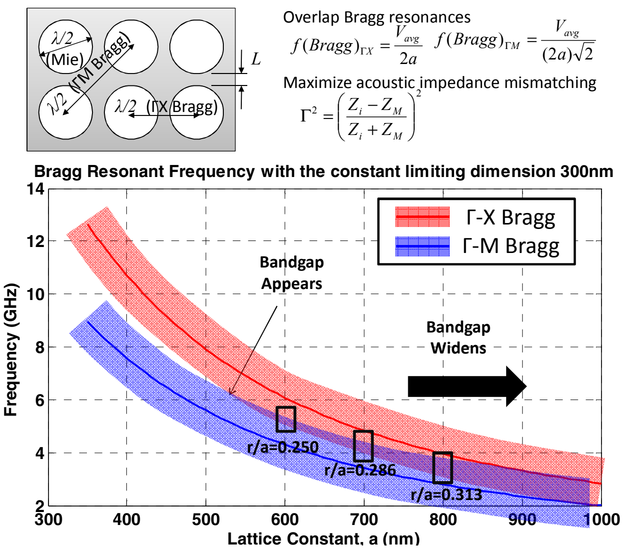

Figure 10. A schematic of hypothetical explanation of bandgap opening effect. At the same limiting dimension, as the lattice constant increases, two Bragg frequencies of square lattice approach each other, therefore widening the bandgap size, which might result in further reduction in thermal conductivity.

This normalized thermal conductivity indicates how much the thermal conductivity is further reduced beyond the contribution from the simple volume reduction effect. For example, Design ID-2 measured k_n=0.805 (see Table 1), which means thermal conductivity is reduced 19.5% additionally, even after taking the volume reduction effect into account. Figure 8 compares the normalized thermal conductivities, k_n, versus the limiting dimensions, L (spacing between adjacent holes) with the same lattice constant, a (hole pitch). For all measured devices, as the limiting dimension decreases, k_n consistently decreases, indicating incoherent phonon scattering plays a significant role in the thermal conductivity reduction.

Figure 9 compares the normalized thermal conductivities, k_n, versus lattice constants, a, at the same limiting dimension, L. As can be seen, k_n consistently decreases as the lattice constant increases even with the same limiting dimension. These differences in k_n indicate that incoherent scattering is not the only mechanism contributing to the reduction in thermal conductivity beyond the volume reduction effect. A schematic in Figure 10 describes a hypothetical explanation for this phenomenon. At the same limiting dimensions, as the lattice constant increases, the two Bragg resonant frequencies, $f_{\Gamma\text{-}X}$ and $f_{\Gamma\text{-}M}$, of the phononic crystals approach each other. Therefore, possibly, at a certain lattice constant, a phononic bandgap opens, and as the lattice constant increases, the bandgap widens. This effect enhances coherent scattering, resulting in a further reduction in thermal conductivity. It is well known that vacuum/solid phononic crystals only open a bandgap at very large filling fractions and that the bandgap widens the more the filling fraction increases [9].

CONCLUSIONS

It has been demonstrated that the thermal conductivity of single crystal silicon can be effectively engineered using lithographically patterned phononic crystals. By introducing sub-micron diameter periodic through holes, the electrical conductivities of the phononic crystal membranes were changed only by the amount of the volume reduction effect, while their thermal conductivities were reduced much further due to the enhanced phonon scattering. This work also elucidates that not only incoherent scattering but also coherent scattering of phonons impact the single crystal silicon thermal conductivity, which has been vague in previous works [10]. These phononic crystals were constructed using only conventional lithography techniques, which not only opens direct applications to many micromachined devices without much modification to their original fabrication process but also allows for their repeatable mass production.

REFERENCES

[1] M. Asheghi, *et al.*, "Thermal conduction in doped …," *Journal of applied physics,* vol. 91, pp. 5079-88, 2002.
[2] M. J. Sinclair, "A high force low area MEMS thermal actuator," in *ITHERM 2000.*, p. 132.
[3] C. M. Jha, *et al.*, "In-Chip Device-Layer Thermal …," in *2006 ASME IMECE*, Chicago, IL, USA, 2006.
[4] T. Huesgen, *et al.*, "Design and fabrication …," *Sens. and Actuators A: Physical,* vol. 145-146, pp. 423-429.
[5] A. J. McGaughey, "Size-dependent model for thin film and nanowire thermal conductivity," *Applied Physics Letters,* vol. 99, p. 131904, 2011.
[6] A. I. Hochbaum, *et al.*, "Enhanced thermoelectric performance …," *Nature,* vol. 451, pp. 163-167, 2008.
[7] F. R. Montero de Espinosa, *et al.*, "Ultrasonic Band Gap in a Periodic Two-Dimensional Composite," *Phys. Rev. Lttrs.,* vol. 80, pp. 1208-1211, 1998.
[8] R. H. Olsson III and I. El-Kady, "Microfabricated phononic crystal devices …," *Measurement Science and Technology,* vol. 20, p. 012002, 2009.
[9] C. M. Reinke, *et al.*, "Realization of optimal bandgaps in …," *Appl. Phys. Lttrs.,* vol. 98, pp. 061912-3, 2011.
[10] J. Tang, *et al.*, "Holey Silicon as an Efficient ...," *Nano Letters,* vol. 10, pp. 4279-4283, 2010/10/13 2010.

CONTACT

*B. Kim, tel: +1-505-8445104; bonkim@sandia.gov